Metabolomics Coupled with Proteomics Advancing Drug Discovery toward More Agile Development of Targeted Combination Therapies*⁃Ⓢ

Xijun Wang‡§, Aihua Zhang‡, Ping Wang‡, Hui Sun¶, Gelin Wu‡, Wenjun Sun‡, Haitao Lv‡, Guozheng Jiao‡, Hongying Xu‖, Ye Yuan‡, Lian Liu‡, Dixin Zou‡, Zeming Wu‡, Ying Han‡, Guangli Yan‖, Wei Dong‡, Fangfang Wu¶, Tianwei Dong‡, Yang Yu‡, Shuxiang Zhang‡, Xiuhong Wu‡, Xin Tong‡, and Xiangcai Meng‡

To enhance the therapeutic efficacy and reduce the adverse effects of traditional Chinese medicine, practitioners often prescribe combinations of plant species and/or minerals, called formulae. Unfortunately, the working mechanisms of most of these compounds are difficult to determine and thus remain unknown. In an attempt to address the benefits of formulae based on current biomedical approaches, we analyzed the components of Yinchenhao Tang, a classical formula that has been shown to be clinically effective for treating hepatic injury syndrome. The three principal components of Yinchenhao Tang are *Artemisia annua* L., *Gardenia jasminoids* Ellis, and *Rheum Palmatum* L., whose major active ingredients are 6,7-dimethylesculetin (D), geniposide (G), and rhein (R), respectively. To determine the mechanisms underlying the efficacy of this formula, we conducted a systematic analysis of the therapeutic effects of the DGR compound using immunohistochemistry, biochemistry, metabolomics, and proteomics. Here, we report that the DGR combination exerts a more robust therapeutic effect than any one or two of the three individual compounds by hitting multiple targets in a rat model of hepatic injury. Thus, DGR synergistically causes intensified dynamic changes in metabolic biomarkers, regulates molecular networks through target proteins, has a synergistic/additive effect, and activates both intrinsic and extrinsic pathways. *Molecular & Cellular Proteomics 12: 10.1074/mcp.M112.021683, 1226–1238, 2013.*

Currently, a paradigm shift is occurring in that there is a new focus on agents that modulate multiple targets simultaneously, rather than working at the level of single protein molecules (1). Multiple-target approaches have recently been employed to design medications that are used to treat atherosclerosis, cancer, depression, psychosis, and neurodegenerative diseases (2). During the past few years, the pharmaceutical industry has seen a shift from the "one disease, one target, one drug" and "one drug fits all" approaches to the pursuit of combination therapies that include more than one active ingredient (3, 4). Because of the complexity of medicine, treatment protocols should be carefully designed, and prescriptions must be carefully developed to successfully fight a given disease. A growing body of evidence has demonstrated that treating illnesses such as human acute promyelocytic leukemia (5, 6), cancer (7), HIV (8), chronic hepatitis C (9), and diabetic nephropathy (10) with treatment regimens that use multiple drugs for combination therapy and related mechanisms usually amplifies the therapeutic efficacy of each agent, yielding maximum therapeutic efficacy with minimal adverse effects (11). Such developments represent a triumph for modern medicine and provide fertile ground for modern drug development (12, 13).

Interestingly, traditional Chinese medicine (TCM),[1] which is a unique medical system that assisted the ancient Chinese in dealing with disease, has advocated combinatorial therapeutic strategies for 2,500 years using prescriptions called formulae (14). Typically, formulae consist of several kinds of crude drugs that originate from medicinal plants, animals, or minerals; one represents the principal component and is called the monarch drug in TCM, and the others serve as

From the ‡National TCM Key Lab of Serum Pharmacochemistry, Key Lab of Chinmedomics, Heilongjiang University of Chinese Medicine and Key Pharmacometabolomic Platform of Chinese Medicines, Heping Road 24, Harbin 150040, China; ¶Department of Pharmaceutical Analysis, Heilongjiang University of Chinese Medicine, Heping Road 24, Harbin 150040, China; ‖Research Center of Chinese Medicine, Heilongjiang University of Chinese Medicine, Heping Road 24, Harbin 150040, China

[1] The abbreviations used are: D, 6,7-dimethylesculetin; DA, discriminant analysis; G, geniposide; HI, hepatic injury; OPLS, orthogonal projection to latent structures; PCA, principal components analysis; R, rhein; TCM, traditional Chinese medicine; UPLC-HDMS, ultra-performance liquid chromatography–high definition mass spectrometry; YCHT, Yinchenhao Tang.

adjuvant components that facilitate the delivery of the principal component to the disease site within the body. More specifically, according to the rules of TCM theory, the famous formulae include four elements: the monarch (which plays the most important role in the formula), the minister (which increases the effectiveness of the monarch herb), the assistant (which helps the monarch and minister herbs reach their target positions), and the servant (which can reduce the adverse effects and/or increase the potency of the whole formula). In formulae, the herbs work together harmoniously to achieve an ideal therapeutic outcome. Therapeutic regimens that include more than one active ingredient are commonly used clinically in Chinese medicine (15). The therapeutic efficacy of TCM is usually attributed to its synergistic properties, its capacity for minimizing adverse reactions, or its improved therapeutic efficacy. Synergism is a core principle of traditional medicine, or ethnopharmacology, and plays an essential role in improving the clinical efficacy of TCM. It is believed, at least in regard to some formulae, that multiple components can hit multiple targets and exert synergistic therapeutic effects (14). A scientific explanation for this type of synergy would certainly promote the reasonable and effective application of TCM and help to encourage rational approaches to the safe combination of healthcare systems from various cultures. Multidrug combinations are increasingly important in modern medicine (16–18). However, the precise mechanisms through which formulae function are poorly understood and must be addressed using a molecular approach.

Yinchenhao Tang (YCHT), which was recorded in *Shanghanlun*, a classic resource on TCM written by Zhongjing Zhang (150–215 A.D.), is one of the most famous Chinese herbal formulae. YCHT consists of *Artemisia annua* L. (the monarch herb), *Gardenia jasminoides* Ellis (the minister herb), and *Rheum Palmatum* L. (the assistant and servant herb) and has been used for more than a thousand years to treat jaundice and liver disorders (19). Pharmacological studies and clinical practice have shown that it can be used clinically to treat cholestasis, hepatitis C, primary biliary cirrhosis, liver fibrosis, and cholestatic liver diseases (20, 21). Our previous study showed that YCHT contains 45 compounds, 21 of which were detected in rat plasma (22). The compatibility of the different compounds in YCHT and the effect on the absorption of these 19 compounds were investigated (23). Interestingly, dimethylesculetin (D) has been shown to be effective in treating hepatic injury (HI) by exerting hepatoprotectivity, and it contributes directly to the therapeutic effect of YCHT (24). Geniposide (G), a primary component of the fruits of *Gardenia jasminoids* Ellis, exhibits various pharmacological properties, including antioxidant, anti-inflammatory, and hepato-protective effects (25–27). Intriguingly, a recent study showed that rhein (R), a metabolite of anthranoids and a major component of *Rheum Palmatum* L., helps to ameliorate liver fibrosis (28–30). Studies indicate that D, G, and R have all been used as marker compounds in quality control for YCHT (31). It is noteworthy that a previous study reported the synergistic effects of DGR based on the pharmacokinetics of the main effective constituents of YCHT (32, 33). These results demonstrate the clinical efficacy of DGR and indicate the need for further research regarding the mechanics of this formula.

It has been proposed that DGR-based combination treatment for HI produces a synergistic effect. However, although much is known regarding the interactions among D, G, and R at pharmacokinetic sites, there is little knowledge regarding the compound's synergistic properties. Understanding the synergistic effects of DGR represents an even greater challenge because multilayered regulation might be involved, with the three compounds having overlapping but distinct target properties. In order to gain insight into the complex biochemical mechanisms that underlie this effective HI therapy, we conducted an investigation incorporating advanced technologies using metabolomic, proteomic, and biochemical analyses throughout the treatment process for HI (which has been shown to respond specifically to these agents). In analyzing the formula design in TCM, here we use the treatment of HI with DGR as a working model. D, G, and R—which are derived from *Artemisia annua* L., *Gardenia jasminoids* Ellis, and *Rheum Palmatum* L., respectively—were used as the active compounds in YCHT, and the efficacy and mechanisms of the DGR combination as used to treat HI were tested both *in vivo* and *in vitro*. This is the first study that investigates the unique synergistic effect of combination dosing and provides support for the popular view that traditional Chinese formulae require multiple components to exert their combined effects.

MATERIALS AND METHODS

Reagents—Acetonitrile (HPLC grade) was purchased from Merck (Darmstadt, Germany). Methanol (HPLC grade) was purchased from Fisher (USA). Distilled water was purchased from Watson's Food & Beverage Co., Ltd. (Guangzhou, China), and formic acid (HPLC grade) was purchased from the Beijing Reagent Company (Beijing, China). Leucine enkephalin was purchased from Sigma-Aldrich, and carbon tetrachloride (CCl_4) was purchased from the Chemicals Factory (Tianjin, China). Glycerol was supplied by the Chemicals Factory. Other chemicals, except as noted, were analytical grade. D, G, and R were isolated within our laboratory and identified via spectral analyses, primarily NMR and MS. After identification, the substances were further purified via HPLC to yield authorized compound with a purity of at least 99%. Freeze-dried YCHT powder was produced by our laboratory. The assay kits were purchased from the Nanjing Jiancheng Biotech Company (Nanjing, China). The other reagents that were used in the two-dimensional electrophoresis were purchased from Bio-Rad.

Animals—Male Wistar rats were bred and maintained in a specific pathogen-free environment. The animals were allowed to acclimatize in metabolic cages for 1 week prior to treatment. The animals were randomly assigned to various groups and treated with D, G, and/or R at the doses indicated in the supplementary material. The experiments were performed with the approval of the Animal Ethics Committee of Heilongjiang University of Chinese Medicine, China. Blood was collected from the hepatic portal vein, and plasma was separated via centrifugation at 4,500 rpm for 5 min at 4 °C, flash frozen in

liquid nitrogen, and stored at −80 °C until the liver function tests and proteomics analyses were performed. Urine was collected daily (at 6:00 a.m.) from the metabolic cages at ambient temperature over the course of the entire procedure and centrifuged at 10,000 rpm at 4 °C for 5 min; the supernatants were then stored frozen at −20 °C for subsequent metabolomic analysis.

Biochemical Analysis—We collected plasma samples in heparinized tubes, kept them on ice for 1 h, and centrifuged them at 4,500 rpm for 15 min at 4 °C. We quantified the levels of plasma alanine transaminase, aspartate transaminase, alkaline phosphatase, glutathione peroxidase, and superoxide dismutase activity and the malondialdehyde, triglyceride, glutamyl transferase, cholesterol, total protein, direct bilirubin, and total bilirubin content using assay kits according to the manufacturer's instructions. The rat livers were removed immediately after plasma collection and stored at −70 °C until analysis.

Histology, Immunohistochemistry, and TUNEL Assay—The livers were fixed in 4% neutral buffered formaldehyde at 4 °C and embedded in paraffin. The liver tissue was stained with H&E for histopathological analysis. Immunohistochemistry was performed using antibodies against Fas and BCL-2. TUNEL staining was performed to detect and quantify apoptotic cells using the *in situ* cell death detection kit. The sections were viewed and photographed using standard fluorescent microscopic techniques.

Metabolomics Analysis—Urine and serum were collected for UPLC-HDMS analysis. For the reversed-phase UPLC analysis, an ACQUITY UPLC BEH C_{18} column (50 mm × 2.1 mm inner diameter, 1.7 μm, Waters Corp., Milford, MA) was used. The column temperature was maintained at 35 °C, the flow rate during the mobile phase was 0.50 ml/min, and the injection volume was fixed at 2.0 μl. Mobile phase A involved the use of 0.1% formic acid in acetonitrile, whereas mobile phase B involved the use of 0.1% formic acid in water. For the urine UPLC-HDMS (Waters Corp., Milford, MA) analysis, the optimal conditions for positive ion mode were as follows: capillary voltage of 2,500 V, desolvation temperature of 350 °C, sample cone voltage of 35 V, extraction cone voltage of 3 V, microchannel plate voltage of 1,600 V, collision energy of 4 eV, source temperature of 110 °C, cone gas flow of 50 l/h, and desolvation gas flow of 600 l/h. A lock mass of leucine enkephalin at a concentration of 200 pg/ml in acetonitrile (0.1% formic acid):H_2O (0.1% formic acid) (50:50, v/v) for positive ion mode ([M+H]$^+$ = 556.2771) was employed via a lock-spray interface. The data were collected in centroid mode, the lock-spray frequency was set at 5 s, and the lock-mass data were averaged over 10 scans. A "purge-wash-purge" cycle was employed when the auto-sampler was used, with 90% aqueous formic acid used for the wash solvent and 0.1% aqueous formic acid used as the purge solvent, which ensured minimal carry-over between injections. The mass spectrometry full-scan data were acquired in the positive ion mode from 100 to 1,000 Da with a 0.1-s scan time. For the plasma UPLC-HDMS analysis, the desolvation gas flow was 600 l/h, and the other parameters were the same as for the urine. The MS data were generated and recorded using MassLynx V4.1 (Waters Corp., Milford, MA), MarkerLynx Application Manager (Waters Corp., Milford, MA) was used for peak detection, and EZinfo 2.0 software (which is included in MarkerLynx Application Manager and can be applied directly) was used for the principal component analysis (PCA), partial least squares–discriminant analysis (PLS-DA), and orthogonal projection to latent structures (OPLS) analysis. "Unsupervised" data were analyzed using PCA, and "supervised" analysis was conducted using PLS-DA and OPLS. Putative markers were extracted from S-plots that were constructed following the analysis using OPLS, and markers were chosen based on their contribution to the variation and correlation within the data set. The processed data were then analyzed using EZinfo 2.0 software. The potential biomarkers were matched with the structure message of metabolites acquired from available biochemical databases, the Human Metabolome Database, and the Kyoto Encyclopedia of Genes and Genomes.

Proteomics Analysis—Two-dimensional polyacrylamide gel electrophoresis tests were performed. Protein spots with more than a 3-fold change in density (paired Student's *t* test yielding $p \leq 0.05$) with consistent increases or decreases were considered as differentially expressed and were selected for further identification via a MALDI-TOF-MS/MS analysis. Details regarding the immobilized pH gradient (IPG)-2-DE and image analysis, MALDI-TOF-MS/MS analysis, and Gene Ontology (GO) functional analysis can be found in the supplementary material. All experiments were performed at least in triplicate to ensure reproducibility.

Statistical Analyses—All statistical analyses were performed using Student's *t* test. Differences with a *p* value of 0.05 or less were considered significant. Assays were performed in triplicate, and the results are expressed as mean ± S.D.

RESULTS

Therapeutic Efficacy of DGR as Indicated by a Rat HI Model—The efficacy of combination therapy with D, G, and R was compared with the efficacy of monotherapy with each of the three components individually in a rat model of HI. There was significant variation between the biochemical indicators for the control and model groups after CCl_4 treatment (supplementary Table S1). This indicates that the HI model successfully replicated the disease. The model group had higher alanine transaminase, aspartate transaminase, alkaline phosphatase, r-glutamyl transferase, triglyceride, total cholesterol (TC), malondialdehyde, total bilirubin, direct bilirubin, and total protein values but had lower levels of superoxide dismutase and glutathione peroxidase than the control animals. Each treatment group was treated back to baseline levels (*i.e.* those of the control group), which demonstrates that these drugs had a therapeutic effect in the rat HI model. Our data show that the DGR combination statistically intensified the therapeutic efficacy relative to the control condition or monotherapy using D, G, or R (supplementary Table S1). Interestingly, the DGR protocol decreased the levels of alanine transaminase, aspartate transaminase, alkaline phosphatase, total bilirubin, direct bilirubin, glutamyl transferase, malondialdehyde, and total protein but increased the levels of glutathione peroxidase, triglyceride, and total cholesterol. These results indicate that DGR combination therapy exerted a synergistic effect and yielded better therapeutic effects than did the approaches that were based on the use of D, G, or R as a single agent. These data provide evidence of the synergy that is created with co-administration. Among the various monotherapies, D showed the most potent therapeutic efficacy. Our data also indicate that D is the principal component of the formula, whereas G and R serve as adjuvant ingredients.

DGR Reduces Histologic Changes and Hepatocyte Apoptosis—To confirm the protective effects of DGR in treating liver tissue damage, histological, TUNEL, and immunohistochemical analyses were performed on liver tissue that was obtained from HI rats and compared with tissue from control rats. Microscopic analyses of H&E- and TUNEL-stained liver
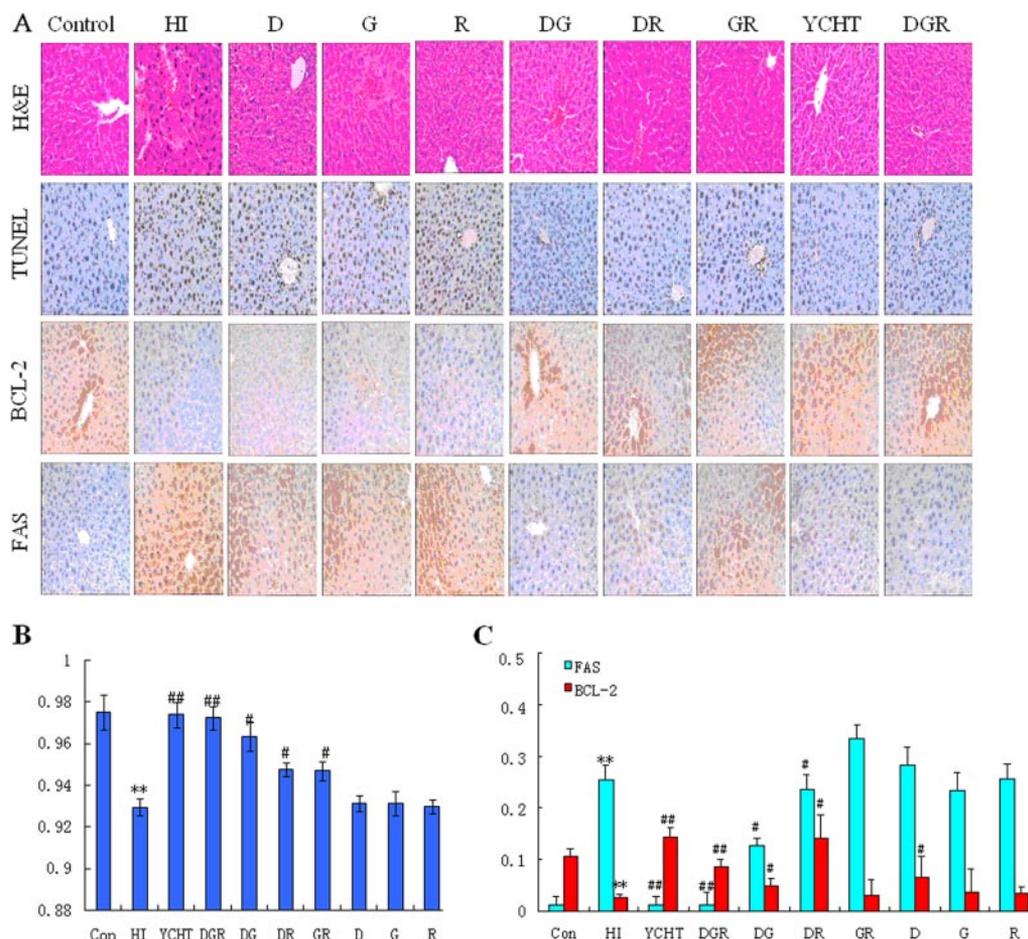
FIG. 1. **Histology, immunohistochemistry, and TUNEL assay.** *A*, representative pictures of liver histopathology (H&E staining), immunohistochemistry, and TUNEL assay of apoptotic hepatocytes after CCL_4 with DGR treatment in rats (original magnification: $\times 200$). *B*, quantitative evaluation of the density of apoptotic hepatocytes using TUNEL staining. *C*, quantitative immunohistochemistry evaluation of the density of Fas- and BCL-2 positive cells. The values are expressed as mean ± S.D. and were compared via analysis of variance. *$p < 0.05$ versus the control group; **$p < 0.01$ versus the control group; #$p < 0.05$ versus the HI group; ##$p < 0.01$ versus the HI group.

sections showed that DGR significantly decreased hepatocyte necrosis, fibrotic area, and hepatocyte apoptosis levels, making them comparable to those in normal liver (Fig. 1*A*). The histopathological examination of liver sections that were stained with H&E revealed numerous apoptotic hepatocytes and the accumulation of massive necrosis with intralobular hemorrhage in the livers of HI rats (Fig. 1*A*). Further analysis revealed multiple and extensive areas of portal inflammation and hepatocellular necrosis in the HI group and a moderate increase in inflammatory cell infiltration. In the portal areas, Kupffer cells were detected within the sinusoids. The degree of necrosis was clearly lower in the CCL_4-treated rats that received YCHT, the DGR combination, or bitherapies using various combinations of D, G, and R (Fig. 1*A*). Minimal hepatocellular necrosis and inflammatory cell infiltration and mild portal inflammation were observed in rats that were treated with either the DGR combination or YCHT as compared with animals that were treated with the control or with monotherapies or biotherapies composed of D, G, and/or R. It is impor-

tant to note that only spotty necrotic hepatocytes were visible in the livers of the DGR-treated rats. Furthermore, the H&E-stained sections indicated that the hepatocyte size had changed in the model rats and that DGR restored normal cell size. These results suggest that the DGR combination prevents the destruction of liver tissue and intensifies therapeutic efficacy.

Next, to investigate further the therapeutic and synergistic properties of the DGR combination, apoptotic hepatocytes were measured using TUNEL staining. Few TUNEL-positive hepatocytes were observed in the livers of CCL_4-treated rats. However, numerous TUNEL-positive hepatocytes ($p < 0.01$) were found in the livers of animals that had been pretreated with DGR, YCHT, or two agents (Fig. 1*A*). Interestingly, the rats that were treated with DGR had the highest density of apoptotic hepatocytes, and the density of apoptotic cells in the rats that were treated with D, G, and R bitherapies was greater than in the rats that were treated with monotherapies (Fig. 1*B*). These results demonstrate that the DG, DR, and RG combinations moderately elevated the density of apoptotic

cells, and the maximum synergistic effect was observed in rats that were treated with the DGR protocol. This is strong evidence that the synergistic effect of D, G, and R occurred at the level of hepatocyte apoptosis. To rigorously test this conclusion, we performed an extensive immunohistochemical analysis using several various antibodies in formalin-fixed, paraffin-embedded liver sections. This analysis was performed with antibodies against Fas and BCL-2 and revealed hepatocytes both in clusters of various sizes in the portal areas and as single cells within the lobules (Fig. 1*C*). Interestingly, a statistically significant difference in the density of FAS- and BCL-2-positive cells was observed between the model and controls. A quantitative immunohistochemical analysis revealed that DG and DR, but not GR, induced a certain degree of (i) up-regulation of BCL-2 (antiapoptotic) ($p < 0.05$) and (ii) decreased density of FAS-positive hepatocytes ($p < 0.05$). Surprisingly, however, the DGR combination induced a much stronger ($p < 0.01$) antiapoptotic effect (Fig. 1*C*). Although G, R, and the GR combination did not dramatically affect the staining pattern, these two compounds facilitated the effects of D (Fig. 1*C*), suggesting that the use of D to up-regulate BCL-2 is more effective when G and R are also used. The oral administration of DGR to HI rats might be more effective at inhibiting the extent of liver necrosis than other treatment regimens. The immunohistochemical assay further confirmed the cooperativity of D and G with R in up-regulating BCL-2 and down-regulating FAS, with the strongest effect resulting from the DGR combination, which supports the rationale of using YCHT to treat HI.

Metabolomic Multivariate Analysis—Using a Waters AC-QUITY UPLC system together with a Waters Micromass quadrupole-time-of-flight Micro Synapt High Definition Mass Spectrometer (UPLC-HDMS) under optimal conditions as described in the supplemental material, the representative base peak intensity chromatograms of the urine or plasma samples that were collected from representative rats from each group were obtained, and these are presented in Figs. 2*A* and 2*B*. The low-molecular-mass metabolites were well separated at 11 min because of the minor particles (sub-1.7 μm) of UPLC. PCA, PLS, and OPLS-DA were used to classify the metabolic phenotypes and identify the differentiating metabolites. Analysis of the OPLS-DA score plots identified the control and HI rats based on differences in their metabolites, suggesting that their metabolic profiles significantly changed as a result of CCL_4 administration (Fig. 2*C*). The PLS-DA loading plots displayed variables that were positively correlated with the score plots (Fig. 2*D*). S-plots and VIP-value plots were combined for the structural identification of the biomarkers (Fig. 2*E*). For example, this information for 2-((hexyloxy)carbonyloxy)benzoic acid is displayed in Fig. 2*F*. Finally, potential biomarkers of significant contributions were identified, with 20 and 12 in the urine and plasma, respectively (Fig. 3 and supplementary Table S2). As seen in Fig. 4 and the supplementary Materials and Methods section, putative metabolic pathways were identified in the HI rats based on changes in the intermediates during substance metabolism.

DGR Causes Synergistic Effects: Trajectory Analysis of HI Rats—In this study, a model of HI rats was constructed, and the dynamic metabolic profiles of treated rats with various outcomes were investigated using UPLC-HDMS and multivariate statistical analysis. With regard to PCA, as shown in Figs. 5*A*–5*C*, the control and model groups were significantly different after CCL_4 treatment, which validates the HI model. Fig. 5*C* shows that YCHT helped prevent HI and maintained the animals in a normal state; there were no distinct clustering differences between the control group and the YCHT treatment group. In contrast, distinct clustering differences were observed between the model group and the groups that received either monotherapy or bitherapy using D, G, and/or R; each dosing regimen returned the values to their baseline levels (*i.e.* those of the control group), but the DGR combination further enhanced this effect. Therefore, the maximum synergistic effect in terms of HI prevention was observed in rats that were treated with the DGR combination as compared with animals that were treated with monotherapy or bitherapy using D, G, and/or R (Figs. 5*A*–5*C*). Similarly, treatment with G or R alone inhibited the occurrence and development of HI, as shown by the clear differences between the control and model groups. Among the monotherapy groups, the group that was treated with D showed the highest level of improvement. This suggests that the therapeutic effect of D on rats with liver injury can be improved by the addition of G and R and provides compelling evidence that the synergistic effect of D, G, and R occurred at the metabolomic level.

DGR Triggers Dynamic Changes in Metabolic Biomarkers—A metabolomic trajectory analysis indicated that each dosing regimen returned the values to their baseline levels (*i.e.* those of the control group), but the maximum synergistic effect in preventing liver injury was observed in rats that were treated with the DGR combination, not in the animals treated with the control or with monotherapy or bitherapy using D, G, and/or R (Fig. 5). These results clearly show that the components of DGR exert a mutual reinforcing effect. This raises the question of how the DGR combination exerts its synergistic effects. To address this question, we further utilized the metabolomics approach to delineate metabolic changes in HI after each treatment. Potential biomarkers were identified, with 20 and 12 in the urine and plasma, respectively (supplementary Table S2). A dynamic change analysis of the levels of metabolic biomarkers was also used to determine whether D, G, and/or R exerted synergistic effects. These metabolites, when identified together, are important to the host's response to HI because they affect energy metabolism, amino acid metabolism, nucleotide metabolism, and lipid metabolism. The metabolic pathways of the biomarkers for the HI model are presented in Fig. 4. The coefficient of variation plots (Fig. 5*D*) for the biomarkers indicating the metabolite concentrations in the DGR group showed the high relative weights of
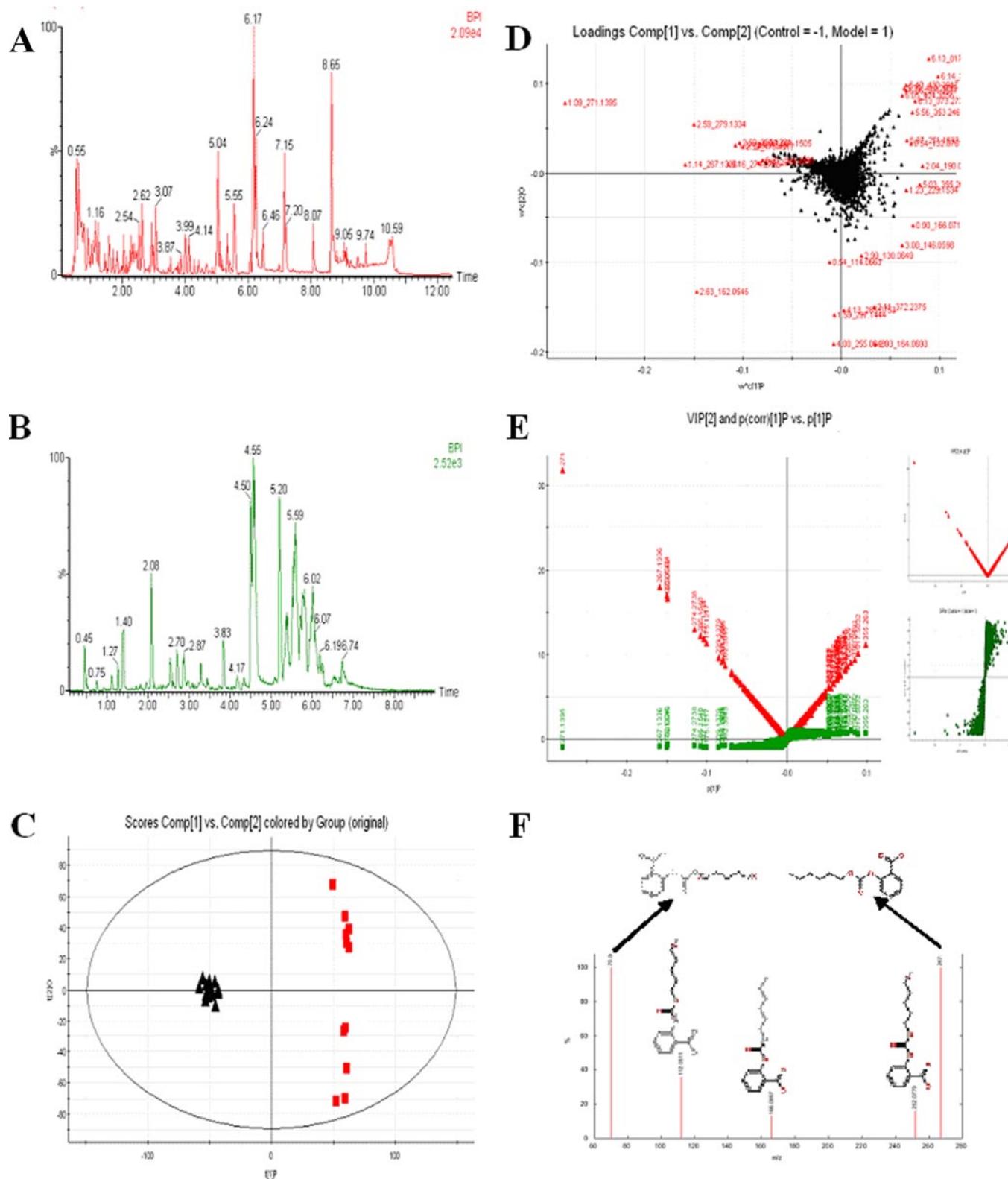
FIG. 2. **Metabolomic multivariate analysis.** *A*, Base peak intensity chromatograms of urine samples. *B*, Base peak intensity chromatograms of plasma samples. *C*, OPLS-DA score plot for the control and HI groups. (▲, control group; ■, model group). *D*, the PLS-DA loading plots for the control and HI groups. *E*, a combination plot of S-plot and VIP values. The red point graph is the VIP value plot, which represents the value of each metabolite. The farther from the origin, the higher the VIP value of the metabolites. *F*, chemical structure and mass fragment information for 2-((hexyloxy) carbonyloxy)benzoic acid.
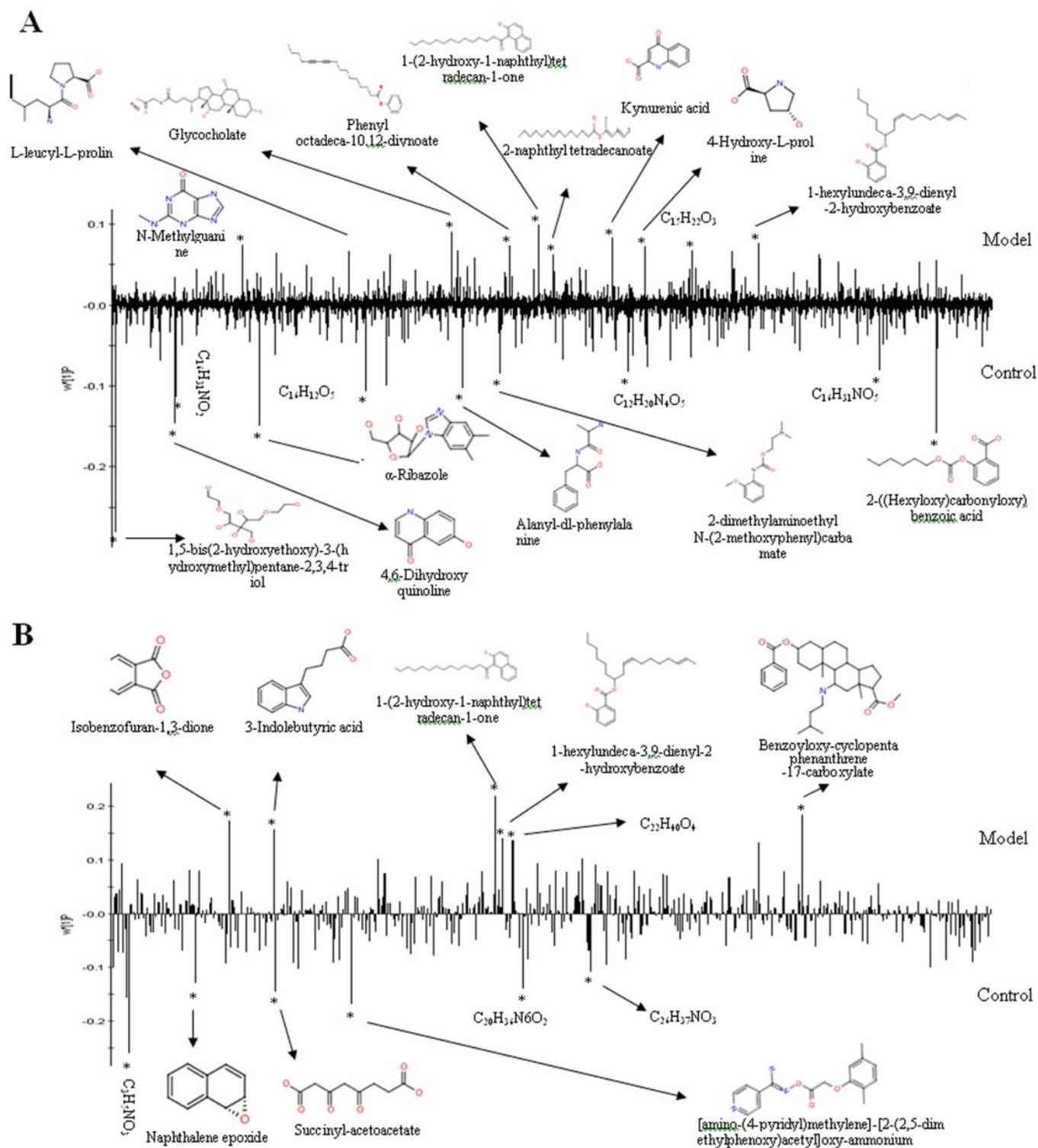
Fig. 3. **Loading plots of OPLS-DA model of potential biomarkers identified.** *A*, urine. *B*, plasma.

these metabolite levels, thereby indicating that they had exerted the greatest effect on HI. Additionally, a dynamic change analysis of the biomarkers further validated the metabolomic findings. Clear differences between the treatment and control groups were observed with each dose.

Interestingly, the maximum synergistic effect in preventing liver injury was observed in the rats that were treated with the DGR protocol, whereas the animals that were treated with monotherapy or bitherapy using D, G, and/or R showed weaker results. Taken together, these results provide a com-
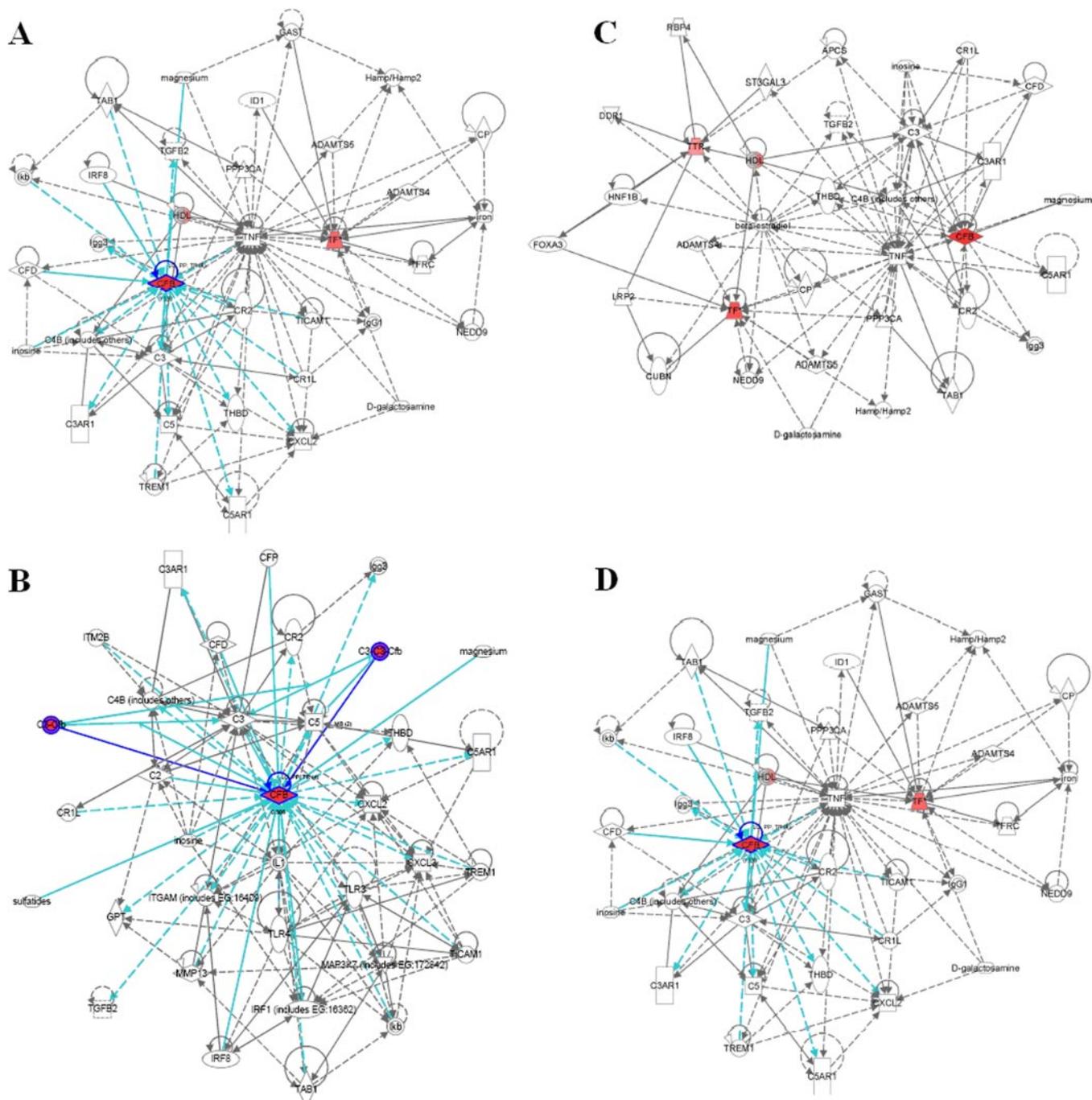
FIG. 4. **Merged network combining major signaling networks associated with the metabolites differentially expressed in the Ingenuity pathway analysis.** *A*, HI group; *B*, D group; *C*, DG group; *D*, DGR group.

prehensive dynamic metabolic profile and serve as the basis for further study of the mechanisms that underlie synergism. Metabolic pathway analysis with IPA software revealed that metabolites that were identified together were important for the host response to HI (Fig. 4). To uncover signal transduction pathways and/or signaling networks associated with the differentially expressed metabolites, the identified metabolites were imported into the IPA software. According to the IPA knowledge base, major signaling networks, comprising 38 nodes, were associated with this set of proteins. The integrated network included differentially expressed metabolites and involved small molecular-transport-associated major signaling pathways.

Proteomic Identification of the Target Proteins for HI—To better understand CCL_4-induced proteins in HI rats, we investigated dynamic proteomic differences between the model
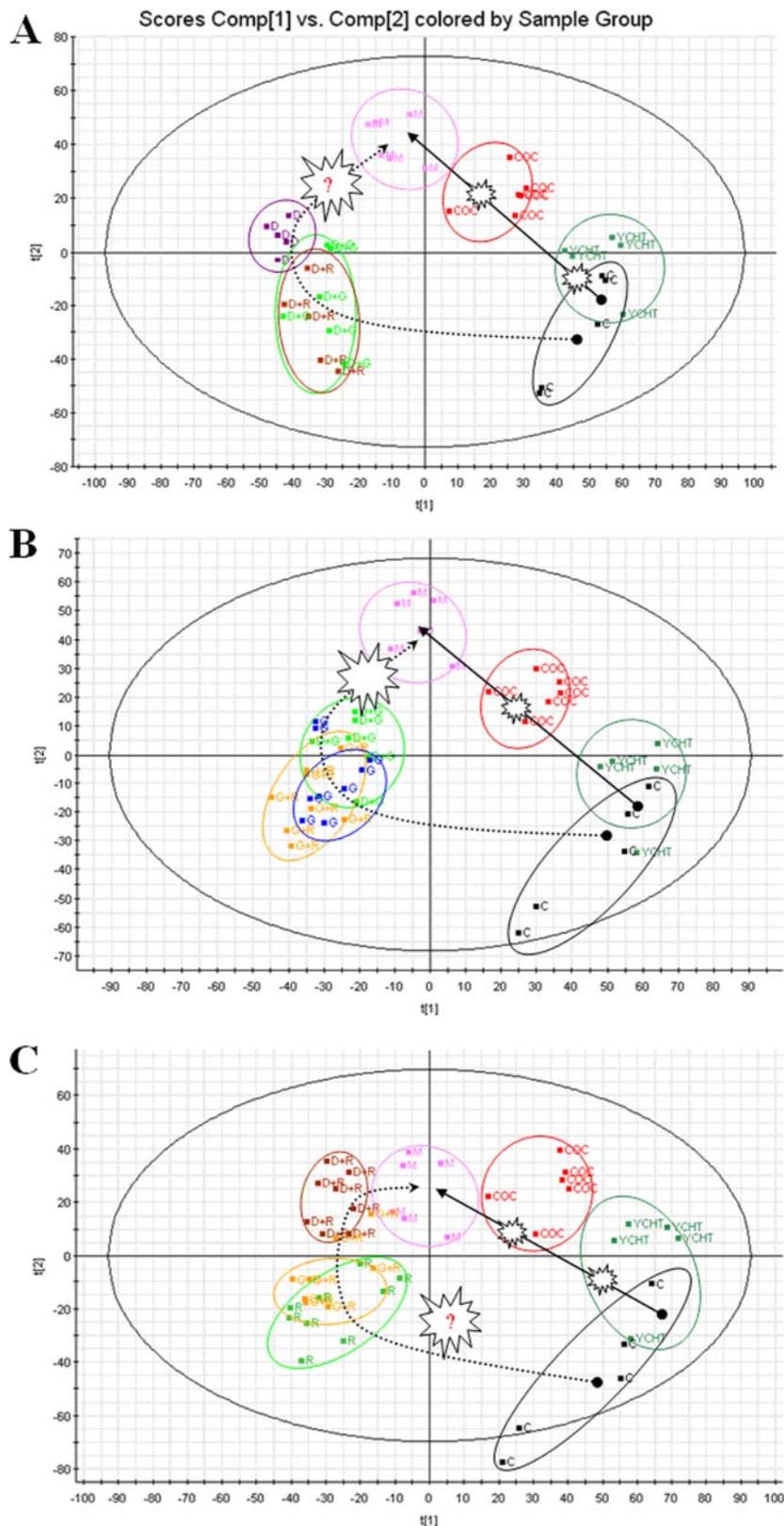
FIG. 5. **DGR causes synergistic effects on trajectory analysis of HI rats.** For each cluster, dotted circles indicate the subject closest to the average user profile within the group. *A*, trajectory analysis of PCA score plots for the HI rats after D treatment. *B*, trajectory analysis of PCA score plots for the HI rats after G treatment. *C*, trajectory analysis of PCA score plots for the HI rats after R treatment. ■C, control; ■M (pink), HI group; ■COC (red), DGR group; ■DG (green); ■DR (brown); ■GR (yellow); ■G (blue); ■D (brown); ■R (green).

and control groups. After the two-dimensional electrophoresis gels had been analyzed, the peptides were extracted from each differentially expressed protein spot using in-gel trypsin digestion, and the proteins were identified using MS/MS. Original images of the silver-stained two-dimensional gels are not shown in the supplementary materials. Representative
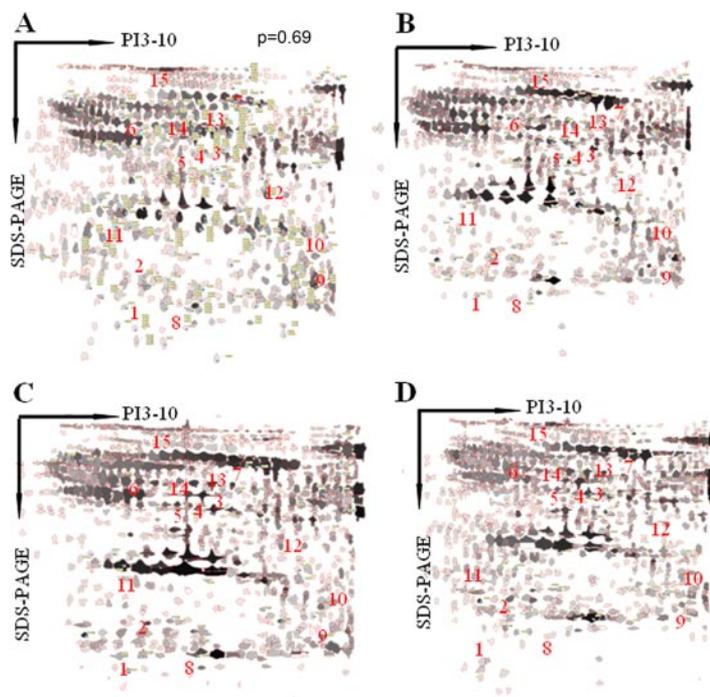
FIG. 6. **Two-dimensional gel electrophoresis representative proteomic maps.** *A*, the control group. *B*, the HI group. *C*, the YCHT-treated group. *D*, the DGR-treated group. The protein spots that are indicated with numbers represent the differentially expressed proteins.

two-dimensional electrophoresis images for the control and model groups are shown in Figs. 6*A* and 6*B*. The results of the MS/MS analysis—including the protein score, coverage, number of identified peptides, and best ion score for each spot—are summarized in supplementary Table S3. Among all of the protein spots that were separated using two-dimensional gel electrophoresis, 42 spots appeared to be significantly changed in percent volume as identified by peptide mass fingerprints that were based on MALDI-TOF-MS/MS and database searching. We found 15 plasma proteins (7 of which were up-regulated and 8 of which were down-regulated) that were expressed in the animal model. The up-regulated proteins in the HI group were Ig kappa chain C, zinc finger protein 407, serotransferrin, haptoglobin, macroglobulin, alpha-1-antitrypsin, and complement factor B. The down-regulated proteins were fibrinogen alpha chain precursor, glyceraldehyde-3-phosphate dehydrogenase, albumin, 2,4-dienoyl-CoA reductase, transthyretin, α-1-inhibitor 3, vitamin D-binding protein, and prothrombin. The synergistically/additively regulated proteins appear to be involved in metabolism, energy production, immunity, chaperoning, antioxidation, and signal transduction. These data help to clarify the molecular mechanisms that underlie the therapeutic and synergistic properties of YCHT.

Functional Analysis of Novel Proteomic Biomarkers—To better understand the molecular mechanisms and relevant pathways that underlie DGR's ability to treat HI at the proteomic level, we employed a proteomics strategy that involved combining two-dimensional gel electrophoresis and MALDI-TOF-MS/MS to perform functional enrichment analysis, with a special focus on the changes in the HI biological

process after each treatment. We found seven and eight target proteins that were up-regulated and down-regulated, respectively, and that were highly specific to the HI model (supplementary Table S3). The detection of these proteins with distinct regulatory patterns provides evidence that novel biomarkers are actively involved in multifunctional pathways that are likely essential for HI. The biological functions of these critical proteins can be sorted into five groups: (i) generation and degradation of the extracellular matrix, including fibrinogen alpha chain precursors and macroglobulin; (ii) the regulation of transcription and translation, as provided by zinc finger proteins; (iii) acute phase reaction and immunity protection, as provided by Ig kappa chain C, alpha-1-antitrypsin, α-1-inhibitor 3, prothrombin, and vitamin D-binding protein; (iv) oxygenation and cell apoptosis, to which 2,4-dienoyl-CoA reductase contributes; and (v) transport and metabolism, as provided by glyceraldehyde-3-phosphate dehydrogenase, haptoglobin, serotransferrin, and transthyretin. The characteristic functions of these differentially expressed proteins were enriched within clusters that were based on biological processes such as immunity, cellular apoptosis, transport, signal transduction, cell growth and proliferation, and metabolism. For example, the modulation of several key members of the immunity cluster was revealed via proteome analysis, as highlighted by Ig kappa chain C, α-1-inhibitor 3, and prothrombin. As expected, currently available HI biomarkers rely on the measurement of substances that are key to the development, transport, and metabolism of HI and thus have unlimited clinical application value in predicting HI. These proteins therefore may be considered as candidates for the further

investigation of synergistic mechanisms and might be potential therapeutic targets for HI.

Synergistic Effects of DGR on the Relative Expression Levels of Target Proteins—Because DGR exerts preferential and synergistic effects on the proteome, it was worthwhile to further investigate the protein expression profiles of the model and of each dosing group using comparative proteomics analysis. We found that a total of 15 target proteins were synergistically/additively modified by DGR based on two-dimensional gels. Figs. 6B, 6C, and 6D show the proteome maps (two-dimensional gel electrophoresis images) for HI, YCHT-treated, and DGR-treated rats, respectively. Supplementary Table S4 summarizes the relative expression levels (in terms of the percent volume) of these proteins. Image analysis revealed 15 differentially expressed proteins ($p < 0.01$ by Student's t test with a fold change > 3.0). For the purpose of protein identification, differentially expressed proteins were isolated from the two-dimensional gel and analyzed using MS after in-gel digestion. Among these proteins, we found a striking number of uniquely HI-associated proteins. All of the details regarding the relative expression levels for the control, model, and dosed rats are provided in supplementary Table S4. For example, the amount of zinc finger protein (spot 2) was 0.1811 in the control and down-regulated to 0.0693 in the model group. We found that both D and G up-regulated the zinc finger protein at the proteomic level, whereas YCHT significantly enhanced zinc finger protein up-regulation (0.1279). Interestingly, the DGR combination induced strong expression (0.1621), reflecting potential therapeutic and synergistic properties of DGR in treating HI. Equally notable is the haptoglobin protein (spot 4), which showed strong up-regulation in the model group and down-regulation in the YCHT, DGR, D, and G groups. In this study, the level of alpha-1-antitrypsin (spot 6) was up-regulated in the model rats relative to controls (indicating its importance in liver injury), down-regulated in the YCHT and DGR groups, and absent (not detectable) in the DG, DR, GR, D, G, and R groups. We found that the expression of the vitamin D-binding protein (spot 14) was slightly increased in the groups that were treated with D (*i.e.* the D, DG, and DR groups) and was dramatically up-regulated in the DGR treatment group. Although G, R, and the GR combination did not exert this significant effect, these two compounds (G and R) enhanced the effects of D, indicating that the expression of the vitamin D-binding protein by D can be further amplified by G and R. This is strong evidence of a synergistic effect of D, G, and R at the proteomic level that occurs by means of coordinated protein expression. These observations indicate that DGR had a synergistic/additive effect on transport, metabolism, and the modulation of immunological processes in HI rats and that these effects were much more pronounced with co-treatment than with any single treatment. These data, together with the biochemical, immunohistochemical, and metabolomic analyses, suggest that D is the principal ingredient in this formula, whereas G and R serve as adjuvant components, and that by hitting multiple targets the DGR combination exerts more profound therapeutic effects than either monotherapy or bitherapy using D, G, and/or R.

DISCUSSION

Currently, in contrast to the traditional focus on single targets, a paradigm shift is occurring that is sparking new interest in agents that modulate multiple targets simultaneously with fewer adverse effects and lower toxicity. Combination medicines with multi-effect pathways and multi-effect targets tend to be more effective than single drugs and might help to address many treatment-related challenges (33). Modern medical therapy has long acknowledged the usefulness of combination therapies that regulate multiple nodes of the disease network simultaneously and have a synergistic effect on the treatment of multifactorial diseases such as acute promyelocytic leukemia and cancer (34–36). However, continued progress will be essential if we are to develop effective, customized multi-drug regimens. TCM, the therapeutic efficacy of which is based on the combined action of a mixture of constituents, offers new treatment opportunities. In recent years, there has been a significant increase in the clinical use of combinatorial intervention in TCM to achieve synergistic interactions that are capable of producing a sufficient effect at low doses. Most Chinese therapeutic herbs that are traditionally used in co-treatment but not mono-treatment series exert significantly better pharmacological effects. However, the precise mechanism of synergistic action remains poorly understood. Based on syndromes and patient characteristics and guided by the theories of TCM, formulae are designed to contain a combination of various kinds of crude drugs that, when combined, will achieve better clinical efficacy. One example is YCHT, whose efficacy in treating HI has recently been well established. Because the means of action of DGR on HI has not been sufficiently investigated, we used an "omics" platform and identified the key mechanisms that underlie the observed effects. To gain insight into the complex biochemical mechanisms of this effective HI therapy, we conducted an investigation that incorporated modern biochemical analyses, immunohistochemistry, metabolomics, and proteomics, analyzing the effects of D, G, R, DG, DR, RG, and DGR treatments on HI. It is well known that CCl_4 is a potent hepatotoxic agent that is rapidly metabolized *in vivo* to the CCl_3 free radical, which subsequently acts on liver cells to covalently conjugate membranous unsaturated lipids, leading to lipid peroxidation; thus, CCl_4 is widely used to model HI in rats. Based on our previous metabolomics findings, we know that YCHT can significantly prevent HI by interfering with the trajectory changes in the biomarkers, exerting an overtly hepatoprotective effect (20, 21). We have now tested the therapeutic and synergistic properties of YCHT that make it an effective treatment for HI using a rat model. We employed UPLC-HDMS, MALDI-TOF-MS/MS, and two-dimensional gel

electrophoresis to systematically analyze the synergism of DGR at the levels of the proteome and metabolome, thereby exploring some of the key molecular mechanisms that underlie these synergistic effects. Our approach extends the well-established concept of combinatorial therapeutics and identifies new potential strands of investigation that involve multicomponent combinations that target multiple pathways.

In this study, we have shown that the combined *in vivo* use of the active components of YCHT (namely, D, G, and R) exerts more profound therapeutic effects than any component used individually in a rat model of HI. DGR significantly intensified the therapeutic efficacy as indicated by our modern biochemical analysis. The immunohistochemical assay further supports the cooperation of D and G with R in up-regulating BCL-2 and down-regulating Fas, with the strongest effect occurring with the DGR combination, thereby supporting the rationale of using YCHT for treating HI. These observations provide mechanistic insight into the synergistic effect. Our metabolomic trajectory analysis indicated that each dosing group could be regulated back to baseline levels (*i.e.* those of the control group), but the maximum synergistic effect on liver injury was observed in rats treated with the DGR combination, as opposed to mono- or bitherapies. These observations support the rationale of this formula wherein the compounds mutually reinforce each other. We also found that DGR activated an array of factors that are involved in energy, amino acid, nucleotide, fatty acid, cofactor, and vitamin metabolism, and we suggest that these effects might form the basis of DGR synergy. This study has indicated that a metabolomics approach can be used to elucidate the synergistic mechanisms employed by TCM. Our study has identified robust biomarkers that are related to HI, with a special focus on the changes in the relative expression levels of target proteins after each treatment. It is important to note that based on our results, DGR targets not only immunity and metabolism but also key regulatory pathways that are used in transport, signal transduction, and cell growth and proliferation, thereby helping to restore the normal function of the liver. Our data will help to indicate the molecular mechanisms of synergism at the proteomic level.

According to the rules of TCM theory, the monarch, minister, assistant, and servant herbs that constitute a formula can work together harmoniously to achieve an ideally synergistic and therapeutic outcome. Understanding the synergistic effects of YCHT represents an even greater challenge than usual. This is because in YCHT, the multilayer regulation structure involves three compounds with overlapping but distinct target properties. However, determining their targets would shed new light on synergism and efficient therapeutic strategies. Although the YCHT formula was designed by TCM doctors in the pre-molecular era, its mode of function can be revealed using modern biochemical analyses. In summary, we have shown that TCM formulae can be analyzed using biomedical and chemical research approaches at the biochemistry, proteome, and metabolome levels. Here, we report that the DGR-based treatment regimen yields encouraging outcomes, reinforcing its potential use as a frontline therapy for HI. This study can be considered as a useful pilot trial in the effort to evaluate traditional formulae on a larger scale and to bridge Western and Eastern medicines in this era of systems biology. Furthermore, these observations indicate that traditional Chinese formulae usually require multiple components to exert their effects, possibly laying the foundation for promising new schemes and patterns of drugs that are derived from TCM.

Ⓢ This article contains supplemental material.

§ To whom correspondence should be addressed: Prof. Xijun Wang, National TCM Key Lab of Serum Pharmacochemistry, Heilongjiang University of Chinese Medicine and Key Pharmacometabolomic Platform of Chinese Medicines, Heping Road 24, Harbin 150040, China. Tel./Fax: +86-451-82110818; E-mail: xijunwangls@126.com.

REFERENCES

1. Drews, J. (2000) Drug discovery: a historical perspective. *Science* **287,** 1960–1964
2. van der Greef, J., Martin, S., Juhasz, P., Adourian, A., Plasterer, T., Verheij, E. R., and McBurney, R. N. (2007) The art and practice of systems biology in medicine: mapping patterns of relationships. *J. Proteome Res.* **6,** 1540–1559
3. Zheng, P. Z., Wang, K. K., Zhang, Q. Y., Huang, Q. H., Du, Y. Z., Zhang, Q. H., Xiao, D. K., Shen, S. H., Imbeaud, S., Eveno, E., Zhao, C. J., Chen, Y. L., Fan, H. Y., Waxman, S., Auffray, C., Jin, G., Chen, S. J., Chen, Z., and Zhang, J. (2005) Systems analysis of transcriptome and proteome in retinoic acid/arsenic trioxide-induced cell differentiation/apoptosis of promyelocytic leukemia. *Proc. Natl. Acad. Sci. U.S.A.* **102,** 7653–7658
4. Yohannes, E., Chang, J., Tar, M. T., Davies, K. P., and Chance, M. R. (2010) Molecular targets for diabetes mellitus-associated erectile dysfunction. *Mol. Cell. Proteomics* **9,** 565–578
5. Wang, Z. Y., and Chen, Z. (2008) Acute promyelocytic leukemia: from highly fatal to highly curable. *Blood* **111,** 2505–2515
6. Zhang, Q. Y., Mao, J. H., Liu, P., Huang, Q. H., Lu, J., Xie, Y. Y., Weng, L., Zhang, Y., Chen, Q., Chen, S. J., and Chen, Z. (2009) A systems biology understanding of the synergistic effects of arsenic sulfide and Imatinib in BCR/ABL-associated leukemia. *Proc. Natl. Acad. Sci. U.S.A.* **106,** 3378–3383
7. Zhang, L., Ren, X., Alt, E., Bai, X., Huang, S., Xu, Z., Lynch, P. M., Moyer, M. P., Wen, X. F., and Wu, X. (2010) Chemoprevention of colorectal cancer by targeting APC-deficient cells for apoptosis. *Nature* **464,** 1058–1061
8. Perelson, A. S., Essunger, P., Cao, Y., Vesanen, M., Hurley, A., Saksela, K., Markowitz, M., and Ho, D. D. (1997) Decay characteristics of HIV-1-infected compartments during combination therapy. *Nature* **387,** 188–191
9. Gao, M., Nettles, R. E., Belema, M., Snyder, L. B., Nguyen, V. N., Fridell, R. A., Serrano-Wu, M. H., Langley, D. R., Sun, J. H., O'Boyle, D. R., 2nd, Lemm, J. A., Wang, C., Knipe, J. O., Chien, C., Colonno, R. J., Grasela, D. M., Meanwell, N. A., and Hamann, L. G. (2010) Chemical genetics strategy identifies an HCV NS5A inhibitor with a potent clinical effect. *Nature* **465,** 96–100
10. Zhang, Z., Zhang, Y., Ning, G., Deb, D. K., Kong, J., and Li, Y. C. (2008) Combination therapy with AT1 blocker and vitamin D analog markedly ameliorates diabetic nephropathy: blockade of compensatory renin in-

crease. *Proc. Natl. Acad. Sci. U.S.A.* **105,** 15896–15901

11. Pibiri, F., Kozikowski, A. P., Pinna, G., Auta, J., Kadriu, B., Costa, E., and Guidotti, A. (2008) The combination of huperzine A and imidazenil is an effective strategy to prevent diisopropyl fluorophosphate toxicity in mice. *Proc. Natl. Acad. Sci. U.S.A.* **105,** 14169–14174

12. Lee, J. Y., Kim, J. Y., Park, G. W., Cheon, M. H., Kwon, K. H., Ahn, Y. H., Moon, M. H., Lee, H. J., Paik, Y. K., and Yoo, J. S. (2011) Targeted mass spectrometric approach for biomarker discovery and validation with nonglycosylated tryptic peptides from N-linked glycoproteins in human plasma. *Mol. Cell. Proteomics* **10,** M111.009290

13. Xiao, T., Ying, W., Li, L., Hu, Z., Ma, Y., Jiao, L., Ma, J., Cai, Y., Lin, D., Guo, S., Han, N., Di, X., Li, M., Zhang, D., Su, K., Yuan, J., Zheng, H., Gao, M., He, J., Shi, S., Li, W., Xu, N., Zhang, H., Liu, Y., Zhang, K., Gao, Y., Qian, X., and Cheng, S. (2005) An approach to studying lung cancer-related proteins in human blood. *Mol. Cell. Proteomics* **4,** 1480–1486

14. Wang, L., Zhou, G. B., Liu, P., Song, J. H., Liang, Y., Yan, X. J., Xu, F., Wang, B. S., Mao, J. H., Shen, Z. X., Chen, S. J., and Chen, Z. (2008) Dissection of mechanisms of Chinese medicinal formula Realgar-Indigo naturalis as an effective treatment for promyelocytic leukemia. *Proc. Natl. Acad. Sci. U.S.A.* **105,** 4826–4831

15. Keith, C. T., Borisy, A. A., and Stockwell, B. R. (2005) Multicomponent therapeutics for networked systems. *Nat. Rev. Drug Discov.* **4,** 71–78

16. Zhang, X. W., Yan, X. J., Zhou, Z. R., Yang, F. F., Wu, Z. Y., Sun, H. B., Liang, W. X., Song, A. X., Lallemand-Breitenbach, V., Jeanne, M., Zhang, Q. Y., Yang, H. Y., Huang, Q. H., Zhou, G. B., Tong, J. H., Zhang, Y., Wu, J. H., Hu, H. Y., de Thé, H., Chen, S. J., and Chen, Z. (2010) Arsenic trioxide controls the fate of the PML-RARalpha oncoprotein by directly binding PML. *Science* **328,** 240–243

17. Wang, X., Zhang, A., and Sun, H. (2012) Future perspectives of Chinese medical formulae: chinmedomics as an effector. *OMICS* **16,** 414–421

18. Chait, R., Craney, A., and Kishony, R. (2007) Antibiotic interactions that select against resistance. *Nature* **446,** 668–671

19. Zhang, Z. J. (2005) *Shanghanlun*, Peo Hygiene, Beijing

20. Zhang, A., Sun, H., Wang, X., Jiao, G., Yuan, Y., and Sun, W. (2012) Simultaneous in vivo RP-HPLC-DAD quantification of multiple-component and drug-drug interaction by pharmacokinetics, using 6,7-dimethylesculetin, geniposide and rhein as examples. *Biomed. Chromatogr.* **26,** 844–850

21. Wang, X., Lv, H., Sun, H., Liu, L., Yang, B., Sun, W., Wang, P., Zhou, D., Zhao, L., Dou, S., Zhang, G., and Cao, H. (2008) Metabolic urinary profiling of alcohol hepatotoxicity and intervention effects of Yin Chen Hao Tang in rats using ultra-performance liquid chromatography/electrospray ionization quadruple time-of-flight mass spectrometry. *J. Pharm. Biomed. Anal.* **48,** 1161–1168

22. Wang, X., Sun, W., Sun, H., Lv, H., Wu, Z., Wang, P., Liu, L., and Cao, H. (2008) Analysis of the constituents in the rat plasma after oral administration of Yin Chen Hao Tang by UPLC/Q-TOF-MS/MS. *J. Pharm. Biomed. Anal.* **46,** 477–490

23. Wang, X., Sun, H., Zhang, A., Jiao, G., Sun, W., and Yuan, Y. (2011) Pharmacokinetics screening for multi-components absorbed in the rat plasma after oral administration traditional Chinese medicine formula Yin-Chen-Hao-Tang by ultra performance liquid chromatography-electrospray ionization/quadrupole-time-of-flight mass spectrometry combined with pattern recognition methods. *Analyst* **136,** 5068–5076

24. Murat Bilgin, H., Atmaca, M., Deniz Obay, B., Ozekinci, S., Taşdemir, E., and Ketani, A. (2011) Protective effects of coumarin and coumarin derivatives against carbon tetrachloride-induced acute hepatotoxicity in rats. *Exp. Toxicol. Pathol.* **63,** 325–330

25. Yin, F., Liu, J., Zheng, X., Guo, L., and Xiao, H. (2010) Geniposide induces the expression of heme oxygenase-1 via PI3K/Nrf2-signaling to enhance the antioxidant capacity in primary hippocampal neurons. *Biol. Pharm. Bull.* **33,** 1841–1846

26. Zheng, X., Yang, D., Liu, X., Wang, N., Li, B., Cao, H., Lu, Y., Wei, G., Zhou, H., and Zheng, J. (2010) Identification of a new anti-LPS agent, geniposide, from Gardenia jasminoides Ellis, and its ability of direct binding and neutralization of lipopolysaccharide in vitro and in vivo. *Int. Immunopharmacol.* **10,** 1209–1219

27. Ma, T., Huang, C., Zong, G., Zha, D., Meng, X., Li, J., and Tang, W. (2011) Hepatoprotective effects of geniposide in a rat model of nonalcoholic steatohepatitis. *J. Pharm. Pharmacol.* **63,** 587–593

28. Guo, M. Z., Li, X. S., Xu, H. R., Mei, Z. C., Shen, W., and Ye, X. F. (2002) Rhein inhibits liver fibrosis induced by carbon tetrachloride in rats. *Acta Pharmacol. Sin.* **23,** 739–744

29. Lin, Y. L., Wu, C. F., and Huang, Y. T. (2008) Phenols from the roots of Rheum palmatum attenuate chemotaxis in rat hepatic stellate cells. *Planta Med.* **74,** 1246–1252

30. Sheng, X., Wang, M., Lu, M., Xi, B., Sheng, H., and Zang, Y. Q. (2011) Rhein ameliorates fatty liver disease through negative energy balance, hepatic lipogenic regulation, and immunomodulation in diet-induced obese mice. *Am. J. Physiol. Endocrinol. Metab.* **300,** E886–E893

31. Wang, X., Lv, H., Sun, H., Jiang, X., Wu, Z., Sun, W., Wang, P., Liu, L., and Bi, K. (2008) Quality evaluation of Yin Chen Hao Tang extract based on fingerprint chromatogram and simultaneous determination of five bioactive constituents. *J. Sep. Sci.* **31,** 9–15

32. Zhang, A., Sun, H., Yuan, Y., Sun, W., Jiao, G., and Wang, X. (2011) An in vivo analysis of the therapeutic and synergistic properties of Chinese medicinal formula Yin-Chen-Hao-Tang based on its active constituents. *Fitoterapia* **82,** 1160–1168

33. Wang, X., Zhang, A., Han, Y., Wang, P., Sun, H., Song, G., Dong, T., Yuan, Y., Yuan, X., Zhang, M., Xie, N., Zhang, H., Dong, H., and Dong, W. (2012) Urine metabolomics analysis for biomarker discovery and detection of jaundice syndrome in patients with liver disease. *Mol. Cell. Proteomics* **1,** 370–380

34. Hyung, S. W., Lee, M. Y., Yu, J. H., Shin, B., Jung, H. J., Park, J. M., Han, W., Lee, K. M., Moon, H. G., Zhang, H., Aebersold, R., Hwang, D., Lee, S. W., Yu, M. H., and Noh, D. Y. (2011) A serum protein profile predictive of the resistance to neoadjuvant chemotherapy in advanced breast cancers. *Mol. Cell. Proteomics* **10,** M111.011023

35. Zhang, M., Yao, Z., Dubois, S., Ju, W., Müller, J. R., and Waldmann, T. A. (2009) Interleukin-15 combined with an anti-CD40 antibody provides enhanced therapeutic efficacy for murine models of colon cancer. *Proc. Natl. Acad. Sci. U.S.A.* **106,** 7513–7518

36. Celis, J. E., Gromov, P., Cabezón, T., Moreira, J. M., Friis, E., Jirström, K., Llombart-Bosch, A., Timmermans-Wielenga, V., Rank, F., and Gromova, I. (2008) 15-prostaglandin dehydrogenase expression alone or in combination with ACSM1 defines a subgroup of the apocrine molecular subtype of breast carcinoma. *Mol. Cell. Proteomics* **7,** 1795–1809